Acta Mech 224, 1–15 (2013)
DOI 10.1007/s00707-012-0724-y

J. Shivakumar · M. H. Ashok · M. C. Ray

Active control of geometrically nonlinear transient vibrations of laminated composite cylindrical panels using piezoelectric fiber reinforced composite

Received: 21 September 2011 / Revised: 4 August 2012 / Published online: 6 October 2012

Abstract This paper addresses the analysis of active constrained layer damping **(ACLD)** of geometrically nonlinear transient vibrations of laminated thin composite cylindrical panels using piezoelectric-fiber-reinforced composite **(PFRC)** materials. The constraining layer of the ACLD treatment is considered to be made of the **PFRC** materials. The Golla–Hughes–McTavish **(GHM)** method has been implemented to model the constrained viscoelastic layer of the ACLD treatment in time domain. The Von Kármán type-nonlinear strain-displacement relations and a simple first-order shear deformation theory are used for deriving this electromechanical coupled problem. A three-dimensional finite element (**FE**) model of smart composite panels integrated with the patches of such **ACLD** treatment has been developed to demonstrate the performance of these patches on enhancing the damping characteristics of thin symmetric and antisymmetric laminated cylindrical panels in controlling the geometrically nonlinear transient vibrations. The numerical results indicate that the **ACLD** patches significantly improve the damping characteristics of both symmetric and antisymmetric panels for suppressing the geometrically nonlinear transient vibrations of the panels. The effect of the shallowness angle of the panels on the control authority of the patches has also been investigated.

1 Introduction

The use of piezoelectric material as distributed actuators and/or sensors for developing high-performing lightweight flexible structures possessing self-controlling and self-sensing capabilities is prevalent and has attracted the attention of several researchers from the past several years [1–18]. These lightweight flexible structures when coupled with the layer/patches of piezoelectric materials acting as distributed sensors and/or actuators are customarily known as "smart structures." Because of the low magnitudes of the piezoelectric coefficients of the existing monolithic piezoelectric materials, a large control voltage is required to achieve significant control of smart structures. In an endeavor to improve the performance of the existing monolithic piezoelectric materials, Baz [19] developed the active constrained layer damping (**ACLD**) treatment. The unwanted vibrations of the substrate structure can be damped out by adding **ACLD** treatment to it. It is established that significant amount of vibration energy is dissipated by the viscoelastic layer undergoing transverse shear deformations. As the

J. Shivakumar
Chhattisgarh Engineering College, Durg 491001, Chhattisgarh, India
E-mail: jskcec@gmail.com

M. H. Ashok (✉)
Maratha Mandal Engineering College, Belgaum, Karnataka, India
E-mail: ashokmh@gmail.com

M. C. Ray
Mechanical Engineering Department, IIT Kharagpur, Kharagpur 721302,
West Bengal, India

constraining layer of the activated **ACLD** treatment increases the passive transverse shear deformation of the viscoelastic constrained layer, the **ACLD** treatment improves the overall damping characteristics of the flexible structures over its passive counterpart. Since the control effort necessary to increase the shear deformation of the viscoelastic layer is compatible with the low control authority of monolithic piezoelectric materials, the piezoelectric materials perform much better to attenuate the vibration of smart structures when they are used as active constraining layer of the **ACLD** treatment than when they are used alone as distributed actuators. **ACLD** treatment provides the attributes of both passive and active damping occurring simultaneously and has been extensively used for efficient and reliable active control of flexible structures [19–25]. The analysis of **ACLD** of laminated thin composite panels using vertically/obliquely reinforced 1–3 piezocomposite materials as the material of the constraining layer of the **ACLD** treatment is carried out [26]. Further, Ray and his co-worker [27] developed a new class of smart composite material, piezofiber-reinforced composite material **(PFRC)** where in piezofibers are aligned horizontally, and they demonstrated the improvement in active control of smart structures by exploiting the in-plane actuation of the distributed actuator. Also, they demonstrated the use of the piezoelectric-fiber-reinforced composites (**PFRC**) as the constraining layer in the **ACLD** treatment for the purpose of active control of vibrations of flexible structures [28]. Later, the use of **ACLD** treatment for controlling the geometrically nonlinear vibrations of flexible structures has been studied. The analysis of **ACLD** of geometrically nonlinear transient vibrations of thin composite plates using horizontally reinforced piezofiber composite material is carried out [29]. Panda and Ray [30] carried out the same for active damping of nonlinear vibrations of functionally graded plates. Subsequently, Ray and his co-worker studied the performance of the vertically reinforced 1–3 **PZC** as the material of the constraining layer of the **ACLD** treatment for active damping of geometrically nonlinear vibrations of composite structures [31–33]. The study on geometrically nonlinear analysis of piezolaminated shallow shells is available in the literature [33–35]. More recently, investigation of performance of the vertically/obliquely reinforced **PZC** as the material of the constraining layer of the **ACLD** treatment for active damping of nonlinear vibrations of shallow shells has been carried out [33]. So far, no work is available till today concerning the **ACLD** of geometrically nonlinear vibrations of laminated composite shallow shells using horizontally reinforced piezofiber composite material such that the in-plane actuation can be utilized for active damping.

This paper addresses the geometrically nonlinear vibration control of smart laminated composite panels using the patches of **ACLD** treatment. The constraining layer of the **ACLD** treatment is made of horizontally reinforced **PFRC** material. A three-dimensional finite element (**FE**) model has been developed to investigate the performance of this composite for developing distributed actuators of smart laminated composite panels. The viscoelastic shear layer is modeled using Golla–Hughes–McTavish **(GHM)** method, which is a time-domain approach. Both symmetric and antisymmetric laminated substrates are considered for presenting the numerical results. The effect of shallowness angle on the nonlinear transient response analysis also has been addressed using the proposed finite element model.

2 Finite element model

Figure 1 illustrates the laminated cylindrical composite panel made of **N** orthotropic layers. The length, circumferential width, thickness, average radius and shallowness angle of the panel are denoted by $\mathbf{a}$, $\mathbf{s}$, $\mathbf{h}$, $\mathbf{R}$ and $\boldsymbol{\phi}$, respectively. The top surface of the panel is integrated with the two rectangular patches of **ACLD** treatment. The constraining layer of the **ACLD** treatment is made of the **PFRC** material in which the fibers are unidirectionally aligned and parallel to the plane of the panel, and its constructional feature is also schematically demonstrated in Fig. 1. The thickness of the **PFRC** layer is $\mathbf{h_p}$ and that of the viscoelastically constrained layer of the **ACLD** treatment is $\mathbf{h_v}$. The mid-plane of the substrate panel is considered as the reference plane. The origin of the curvilinear laminate coordinate system $(\mathbf{x}, \mathbf{y}, \mathbf{z})$ is located at one corner of the reference plane such that the lines $\mathbf{x} = 0$, $\mathbf{a}$ and $\mathbf{y} = 0$, $\mathbf{s}$ represent the boundaries of the panels. Also, the thickness coordinate $(\mathbf{z})$ of the top and bottom surfaces of any layer is denoted by $\mathbf{h_k} + 1$ and $\mathbf{h_k}$, respectively, with $\mathbf{k}$ denoting the layer number of the layer. The fiber orientation angle in any layer of the substrate panel with respect to the laminate coordinate system is denoted by $\boldsymbol{\theta}$, whereas that in the active constraining layer of the **PFRC** material is denoted by $\boldsymbol{\psi}$. First-order shear deformation theories **(FSDT)** are used to describe the kinematics of deformation of the overall panel integrated with the patches of **ACLD** treatment. Figure 2 describes a schematic representation of the kinematics of deformation based on these theories. As shown in this figure, $\mathbf{u_o}$ and $\mathbf{v_o}$ are the generalized translational displacements of a reference point $(\mathbf{x}, \mathbf{y})$ on the mid-plane $(\mathbf{z} = 0)$ of the substrate composite panel along **x-, y-**axes, respectively; $\boldsymbol{\theta_x}$, $\boldsymbol{\phi_x}$ and $\boldsymbol{\gamma_x}$ are the generalized rotations of the normal to the

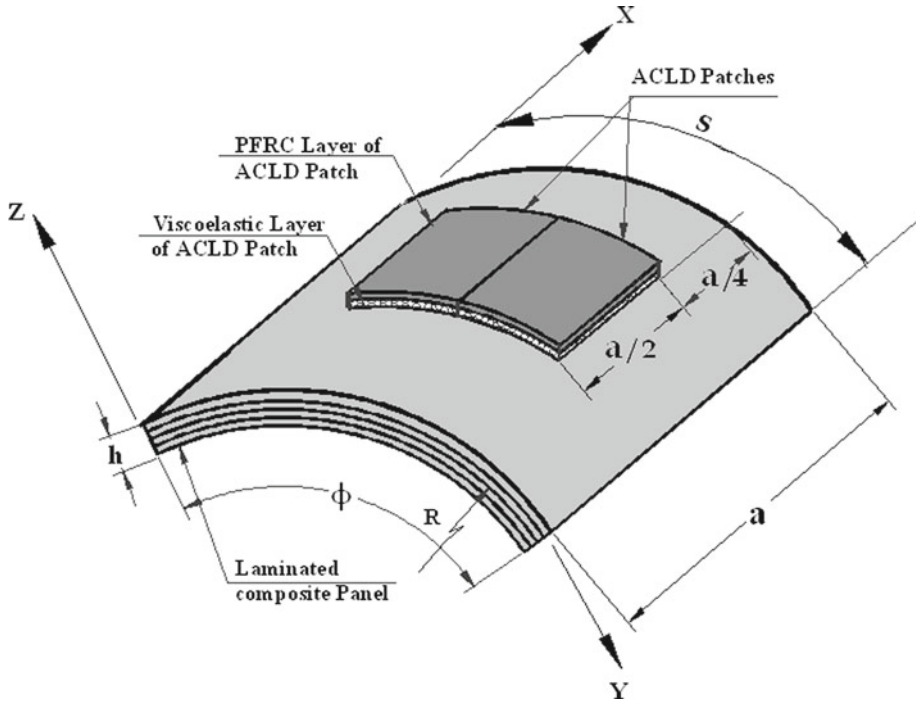

Fig. 1 Schematic representation of laminated composite panel integrated with the patches of ACLD treatment

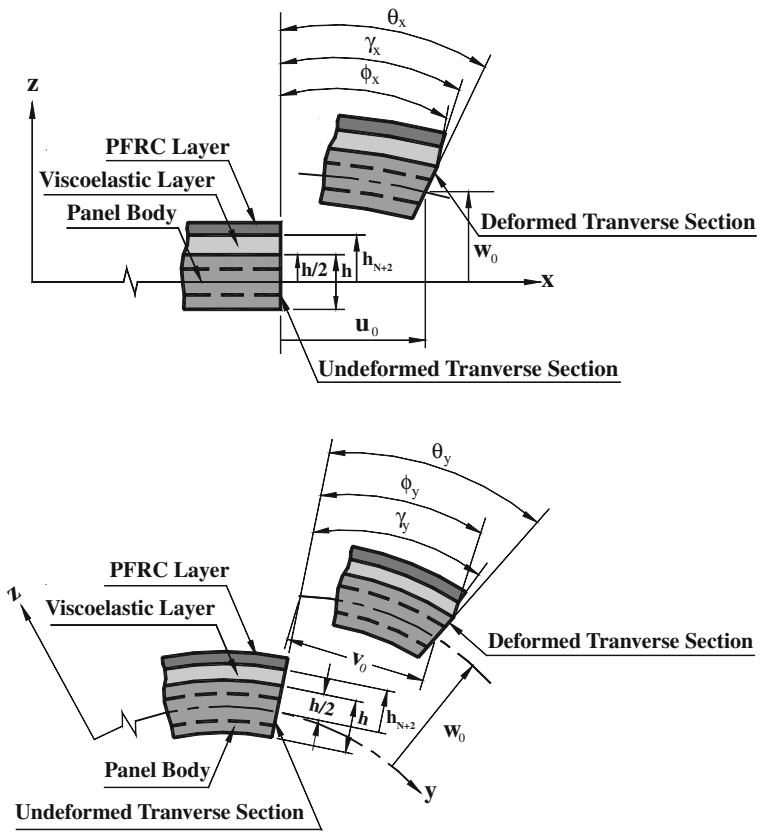

Fig. 2 Schematic diagram of the kinematics of the laminated panel/ACLD system

middle planes of the substrate, viscoelastic layer and the **PFRC** layer, respectively, about the y-axis while the generalized rotations of these normals about the x-axis are denoted, respectively, by $\boldsymbol{\theta_y}$, $\boldsymbol{\phi_y}$ and $\boldsymbol{\gamma_y}$. According to the kinematics of deformation shown in Fig. 2, the displacements **u**, **v** and **w** at any point lying in any layer of the overall panel along **x-**, **y-** and **z**-directions, respectively, can be written as

$$\{\mathbf{d}\} = \{\mathbf{d_t}\} + [\mathbf{Z}]\{\mathbf{d_r}\}, \tag{1}$$

where

$$\{\mathbf{d}\} = [\,\mathbf{u} \quad \mathbf{v} \quad \mathbf{w}]^{\mathbf{T}}, \quad \{\mathbf{d_t}\} = [\,\mathbf{u_o} \quad \mathbf{v_o} \quad \mathbf{w}]^{\mathbf{T}}, \quad \{\mathbf{d_r}\} = [\boldsymbol{\theta_x} \quad \boldsymbol{\theta_y} \quad \boldsymbol{\phi_x} \quad \boldsymbol{\phi_y} \quad \boldsymbol{\gamma_x} \quad \boldsymbol{\gamma_y}]^{\mathbf{T}},$$

$$[\mathbf{Z}] = \begin{bmatrix} \boldsymbol{\lambda}_1(\mathbf{z}) & 0 & \boldsymbol{\lambda}_2(\mathbf{z}) & 0 & \boldsymbol{\lambda}_3(\mathbf{z}) & 0 \\ 0 & \boldsymbol{\lambda}_1(\mathbf{z}) & 0 & \boldsymbol{\lambda}_2(\mathbf{z}) & 0 & \boldsymbol{\lambda}_3(\mathbf{z}) \\ 0 & 0 & 0 & 0 & 0 & 0 \end{bmatrix}, \quad \boldsymbol{\lambda}_1(\mathbf{z}) = \mathbf{z} - \langle \mathbf{z} - \mathbf{h}/2 \rangle,$$

$$\boldsymbol{\lambda}_2(\mathbf{z}) = \langle \mathbf{z} - \mathbf{h}/2 \rangle - \langle \mathbf{z} - \mathbf{h_{N+2}} \rangle \quad \text{and} \quad \boldsymbol{\lambda}_3(\mathbf{z}) = \langle \mathbf{z} - \mathbf{h_{N+2}} \rangle. \tag{2}$$

In Eq. (2), the brackets $\langle\,\rangle$ are used to write the appropriate singularity functions, and thus, Eq. (1) represents the **FSDT** that are applicable, respectively, for the substrate panel, the viscoelastic layer and the **PFRC** layer while maintaining the continuity conditions. To implement the selective integration rule for avoiding the shear locking in thin structures, the state of strains at any point in the overall panel is represented by the two vectors of in-plane strains $\{\boldsymbol{\in_b}\}$ and transverse shear strains$\{\boldsymbol{\in_s}\}$, respectively, and are given by

$$\{\boldsymbol{\in_b}\} = [\,\boldsymbol{\in_x} \quad \boldsymbol{\in_y} \quad \boldsymbol{\in_{xy}}\,]^{\mathbf{T}} \quad \text{and} \quad \{\boldsymbol{\in_s}\} = [\,\boldsymbol{\in_{xz}} \quad \boldsymbol{\in_{yz}}\,]^{\mathbf{T}}, \tag{3}$$

where $\boldsymbol{\in_x}$ and $\boldsymbol{\in_y}$ are the normal strains along the **x-** and **y-**directions, respectively; $\boldsymbol{\in_{xy}}$ is the in-plane shear strain; and $\boldsymbol{\in_{xz}}$ and $\boldsymbol{\in_{yz}}$ are the transverse shear strains. Using the Von Kármán-type nonlinear strain-displacement relations for circular cylindrical panels, the displacement field given by Eqs. (1) and (2), the state of strains at any point in the overall panel can be written in terms of the generalized translational $\{\mathbf{d_t}\}$ and rotational displacements $\{\mathbf{d_r}\}$ as follows:

$$\{\boldsymbol{\in_b}\} = [\mathbf{L_{tb}}]\{\mathbf{d_t}\} + [\mathbf{Z}_1][\mathbf{L_{rb}}]\{\mathbf{d_r}\} + [\mathbf{L_{tnb}}]\{\mathbf{d_t}\} \quad \text{and} \quad \{\boldsymbol{\in_s}\} = [\mathbf{L_{ts}}]\{\mathbf{d_t}\} + [\mathbf{Z}_2]\{\mathbf{d_r}\}, \tag{4}$$

in which the matrices $[\mathbf{Z}_1]$ and $[\mathbf{Z}_2]$ and the different operator matrices are defined as

$$[\mathbf{Z}_1] = [\,\{\boldsymbol{\lambda}_1(\mathbf{z})\}\mathbf{I} \quad \{\boldsymbol{\lambda}_2(\mathbf{z})\}\mathbf{I} \quad \{\boldsymbol{\lambda}_3(\mathbf{z})\}\mathbf{I}\,],$$

$$[\mathbf{Z}_2] = \begin{bmatrix} \boldsymbol{\lambda}_4(\mathbf{z}) & 0 & \boldsymbol{\lambda}_5(\mathbf{z}) & 0 & \boldsymbol{\lambda}_6(\mathbf{z}) & 0 \\ 0 & \boldsymbol{\lambda}_4(\mathbf{z}) - \frac{1}{\mathbf{R}}\boldsymbol{\lambda}_1(\mathbf{z}) & 0 & \boldsymbol{\lambda}_5(\mathbf{z}) - \frac{1}{\mathbf{R}}\boldsymbol{\lambda}_2(\mathbf{z}) & 0 & \boldsymbol{\lambda}_6(\mathbf{z}) - \frac{1}{\mathbf{R}}\boldsymbol{\lambda}_3(\mathbf{z}) \end{bmatrix},$$

$$\boldsymbol{\lambda}_4(\mathbf{z}) = 1 - \langle \mathbf{z} - \mathbf{h}/2 \rangle^{\mathbf{o}}, \quad \boldsymbol{\lambda}_5(\mathbf{z}) = \langle \mathbf{z} - \mathbf{h}/2 \rangle^{\mathbf{o}} - \langle \mathbf{z} - \mathbf{h_{N+2}} \rangle^{\mathbf{o}}, \quad \boldsymbol{\lambda}_6(\mathbf{z}) = \langle \mathbf{z} - \mathbf{h_{N+2}} \rangle^{\mathbf{o}},$$

$$[\mathbf{L_{tb}}] = [\,\mathbf{L}_1 \quad \mathbf{L}_2\,], \quad [\mathbf{L_{tnb}}] = \frac{1}{2}[\mathbf{B}_1][\mathbf{B}_2], \quad \mathbf{L}_1 = \begin{bmatrix} \frac{\partial}{\partial \mathbf{x}} & 0 \\ 0 & \frac{\partial}{\partial \mathbf{y}} \\ \frac{\partial}{\partial \mathbf{y}} & \frac{\partial}{\partial \mathbf{x}} \end{bmatrix}, \quad \mathbf{L}_2 = \begin{bmatrix} 0 & \frac{1}{\mathbf{R}} & 0 \end{bmatrix}^{\mathbf{T}},$$

$$[\mathbf{L_{rb}}] = \begin{bmatrix} \mathbf{L}_1 & \tilde{\mathbf{O}} & \tilde{\mathbf{O}} \\ \tilde{\mathbf{O}} & \mathbf{L}_1 & \tilde{\mathbf{O}} \\ \tilde{\mathbf{O}} & \tilde{\mathbf{O}} & \mathbf{L}_1 \end{bmatrix} \quad \text{and} \quad [\mathbf{L_{ts}}] = \begin{bmatrix} 0 & 0 & \frac{\partial}{\partial \mathbf{x}} \\ 0 & -\frac{1}{\mathbf{R}} & \frac{\partial}{\partial \mathbf{y}} \end{bmatrix},$$

where

$$[\mathbf{B}_1] = \begin{bmatrix} \frac{\partial \mathbf{w_o}}{\partial \mathbf{x}} & 0 \\ 0 & \frac{\partial \mathbf{w_o}}{\partial \mathbf{y}} \\ \frac{\partial \mathbf{w_o}}{\partial \mathbf{y}} & \frac{\partial \mathbf{w_o}}{\partial \mathbf{x}} \end{bmatrix} \quad \text{and} \quad [\mathbf{B}_2] = \begin{bmatrix} 0 & 0 & \frac{\partial}{\partial \mathbf{x}} \\ 0 & 0 & \frac{\partial}{\partial \mathbf{y}} \end{bmatrix}, \tag{5}$$

in which $\mathbf{I}$ and $\tilde{\mathbf{O}}$ appearing in the matrices $[\mathbf{Z}_1]$ and $[\mathbf{L_{rb}}]$ are a (3×3) identity matrix and a (3×2) null matrix, respectively. Corresponding to the description of the state of strains given by Eq. (3), the state of in-plane stresses and the state of transverse shear stresses at any point in the overall panel can be expressed as

$$\{\boldsymbol{\sigma}_\mathbf{b}\} = [\,\boldsymbol{\sigma}_\mathbf{x} \quad \boldsymbol{\sigma}_\mathbf{y} \quad \boldsymbol{\sigma}_\mathbf{xy}\,]^\mathbf{T} \quad \text{and} \quad \{\boldsymbol{\sigma}_\mathbf{s}\} = [\,\boldsymbol{\sigma}_\mathbf{xz} \quad \boldsymbol{\sigma}_\mathbf{yz}\,]^\mathbf{T}, \tag{6}$$

in which $\boldsymbol{\sigma}_\mathbf{x}$ and $\boldsymbol{\sigma}_\mathbf{y}$ are the normal stresses along the **x-** and **y-**directions, respectively; $\boldsymbol{\sigma}_\mathbf{xy}$ is the in-plane shear stress while $\boldsymbol{\sigma}_\mathbf{xz}$ and $\boldsymbol{\sigma}_\mathbf{yz}$ are the transverse shear stresses.

The constitutive relations for the orthotropic layers of the host panel are given by

$$\{\boldsymbol{\sigma}_\mathbf{b}^\mathbf{k}\} = [\bar{\mathbf{C}}_\mathbf{b}^\mathbf{k}]\{\boldsymbol{\epsilon}_\mathbf{b}^\mathbf{k}\} \quad \text{and} \quad \{\boldsymbol{\sigma}_\mathbf{s}^\mathbf{k}\} = [\bar{\mathbf{C}}_\mathbf{s}^\mathbf{k}]\{\boldsymbol{\epsilon}_\mathbf{s}^\mathbf{k}\}, \qquad \mathbf{k} = 1, 2, 3, \ldots \mathbf{N}. \tag{7}$$

The constraining **PFRC** layer will be subjected to the applied electric field ($\mathbf{E_z}$) acting across its thickness (i.e., along the **z-**direction) only. Thus, the constitutive relations for the material of the **PFRC** layer can be expressed as

$$\begin{aligned} \{\boldsymbol{\sigma}_\mathbf{b}^\mathbf{k}\} = [\bar{\mathbf{C}}_\mathbf{b}^\mathbf{k}]\{\boldsymbol{\epsilon}_\mathbf{b}^\mathbf{k}\} - \{\bar{\mathbf{e}}_\mathbf{b}\}\{\mathbf{E_z}\}, \quad \{\boldsymbol{\sigma}_\mathbf{s}^\mathbf{k}\} = [\bar{\mathbf{C}}_\mathbf{s}^\mathbf{k}]\{\boldsymbol{\epsilon}_\mathbf{s}^\mathbf{k}\} \quad \text{and} \\ \mathbf{D_z} = [\bar{\mathbf{e}}_\mathbf{b}^\mathbf{k}]^\mathbf{T}\{\boldsymbol{\epsilon}_\mathbf{b}^\mathbf{k}\} + \bar{\boldsymbol{\varepsilon}}_{33}\mathbf{E_z}, \qquad \mathbf{k} = \mathbf{N} + 2, \end{aligned} \tag{8}$$

in which $\mathbf{D_z}$ is the electric field in the **z-**direction, and $\bar{\boldsymbol{\varepsilon}}_{33}$ is the transformed dielectric constant. The transformed elastic coefficient matrices $[\bar{\mathbf{C}}_\mathbf{b}^\mathbf{k}]$, $[\bar{\mathbf{C}}_\mathbf{s}^\mathbf{k}]$ and the transformed piezoelectric coefficient matrix $\{\bar{\mathbf{e}}_\mathbf{b}\}$ appearing in Eqs. (7) and (8), referred to the laminate coordinate system **(x, y, z)**, are given by

$$[\bar{\mathbf{C}}_\mathbf{b}^\mathbf{k}] = \begin{bmatrix} \bar{\mathbf{C}}_{11}^\mathbf{k} & \bar{\mathbf{C}}_{12}^\mathbf{k} & \bar{\mathbf{C}}_{16}^\mathbf{k} \\ \bar{\mathbf{C}}_{12}^\mathbf{k} & \bar{\mathbf{C}}_{22}^\mathbf{k} & \bar{\mathbf{C}}_{26}^\mathbf{k} \\ \bar{\mathbf{C}}_{16}^\mathbf{k} & \bar{\mathbf{C}}_{26}^\mathbf{k} & \bar{\mathbf{C}}_{66}^\mathbf{k} \end{bmatrix}, \quad [\bar{\mathbf{C}}_\mathbf{s}^\mathbf{k}] = \begin{bmatrix} \bar{\mathbf{C}}_{55}^\mathbf{k} & \bar{\mathbf{C}}_{45}^\mathbf{k} \\ \bar{\mathbf{C}}_{45}^\mathbf{k} & \bar{\mathbf{C}}_{44}^\mathbf{k} \end{bmatrix} \text{ and } \{\bar{\mathbf{e}}_\mathbf{b}\} = \begin{Bmatrix} \bar{\mathbf{e}}_{31} \\ \bar{\mathbf{e}}_{32} \\ \bar{\mathbf{e}}_{36} \end{Bmatrix}. \tag{9}$$

The material of the viscoelastic layer is assumed to be linearly viscoelastic and isotropic. The present study is concerned with the analysis of the laminated cylindrical composite panel undergoing **ACLD** in the time domain. Hence, the viscoelastic material is modeled by the Golla–Hughes–McTavish **(GHM)** method. The constitutive equation for the viscoelastic material is represented in the following Stieltjes integral form [36]:

$$\{\boldsymbol{\sigma}_\mathbf{s}\}_\mathbf{v} = \int_0^\mathbf{t} \mathbf{G}(\mathbf{t} - \boldsymbol{\tau}) \frac{\partial \{\boldsymbol{\epsilon}_\mathbf{s}\}_\mathbf{v}}{\partial \boldsymbol{\tau}} \mathbf{d}\boldsymbol{\tau}, \tag{10}$$

where $\mathbf{G}(\mathbf{t})$ is the relaxation function of the viscoelastic material.

The total potential energy $\mathbf{T_p}$ and the kinetic energy $\mathbf{T_k}$ of the laminated plate coupled with the patches of the **ACLD** treatment can be written as [20]

$$\mathbf{T_p} = \frac{1}{2}\left[\sum_{\mathbf{k}=1}^{\mathbf{N}+2} \int_{\boldsymbol{\Omega}} (\{\boldsymbol{\epsilon}_\mathbf{b}^\mathbf{k}\}^\mathbf{T}\{\boldsymbol{\sigma}_\mathbf{b}^\mathbf{k}\} + \{\boldsymbol{\epsilon}_\mathbf{s}^\mathbf{k}\}^\mathbf{T}\{\boldsymbol{\sigma}_\mathbf{s}^\mathbf{k}\})\mathbf{d}\boldsymbol{\Omega} - \int_{\boldsymbol{\Omega}} \mathbf{E_z}\mathbf{D_z}\mathbf{d}\boldsymbol{\Omega}\right] - \int_\mathbf{A} \{\mathbf{d}\}^\mathbf{T}\{\mathbf{f}\}\mathbf{d}\mathbf{A} \quad \text{and} \tag{11}$$

$$\mathbf{T_k} = \frac{1}{2}\left[\sum_{\mathbf{k}=1}^{\mathbf{N}+2} \int_{\boldsymbol{\Omega}} \boldsymbol{\rho}^\mathbf{k}(\dot{\mathbf{u}}^2 + \dot{\mathbf{v}}^2 + \dot{\mathbf{w}}^2)\mathbf{d}\boldsymbol{\Omega}\right], \tag{12}$$

where $\{\mathbf{f}\}$ is the externally applied surface traction vector acting over a surface area $\mathbf{A}$, and $\boldsymbol{\Omega}$ represents the volume of the concerned domain. $\boldsymbol{\rho}^\mathbf{k}$ is the mass density of the $\mathbf{k}$th layer.

The overall panel has been discretized by eight noded isoparametric quadrilateral elements. Thus, following Eq. (2), the generalized displacement vectors for the $\mathbf{i}$th ($\mathbf{i} = 1, 2, 3, \ldots, 8$) node of the element can be expressed as

$$\{\mathbf{d_{ti}}\} = [\,\mathbf{u_{oi}} \quad \mathbf{v_{oi}} \quad \mathbf{w_i}\,]^\mathbf{T} \quad \text{and} \quad \{\mathbf{d_{ri}}\} = [\,\boldsymbol{\theta}_\mathbf{xi} \quad \boldsymbol{\theta}_\mathbf{yi} \quad \boldsymbol{\phi}_\mathbf{xi} \quad \boldsymbol{\phi}_\mathbf{yi} \quad \boldsymbol{\gamma}_\mathbf{xi} \quad \boldsymbol{\gamma}_\mathbf{yi}\,]^\mathbf{T}. \tag{13}$$

Thus, the generalized displacement vectors at any point within the element can be written as

$$\{\mathbf{d_t}\} = [\mathbf{N_t}]\{\mathbf{d_t^e}\} \quad \text{and} \quad \{\mathbf{d_r}\} = [\mathbf{N_r}]\{\mathbf{d_r^e}\}, \tag{14}$$

wherein the nodal generalized translational displacement vector $\{\mathbf{d}_\mathbf{t}^\mathbf{e}\}$, the nodal generalized rotational displacement vector $\{\mathbf{d}_\mathbf{r}^\mathbf{e}\}$ and the shape function matrices $[\mathbf{N_t}]$ and $[\mathbf{N_r}]$ are given by

$$\begin{gathered}\{\mathbf{d}_\mathbf{t}^\mathbf{e}\} = [\{\mathbf{d_{t1}}\}^\mathbf{T} \quad \{\mathbf{d_{t2}}\}^\mathbf{T} \quad \ldots \quad \{\mathbf{d}_{t8}\}^\mathbf{T}]^\mathbf{T}, [\mathbf{N_t}] = [\mathbf{N_{t1}} \quad \mathbf{N_{t2}} \quad \ldots \quad \mathbf{N_{t8}}],\\ \{\mathbf{d}_\mathbf{r}^\mathbf{e}\} = [\{\mathbf{d_{r1}}\}^\mathbf{T} \quad \{\mathbf{d_{r2}}\}^\mathbf{T} \quad \ldots \quad \{\mathbf{d_{r8}}\}^\mathbf{T}]^\mathbf{T}, [\mathbf{N_r}] = [\mathbf{N_{r1}} \quad \mathbf{N_{r2}} \quad \ldots \quad \mathbf{N_{r8}}],\\ \mathbf{N_{ti}} = \mathbf{n_i I} \quad \text{and} \quad \mathbf{N_{ri}} = \mathbf{n_i I}_2, \end{gathered} \tag{15}$$

where $\mathbf{I}_2$ is a (6×6) identity matrix and $\mathbf{n_i}$ is the shape function of natural coordinates associated with the $\mathbf{i^{th}}$ node of the element. Using the relations given by Eq. (14) in Eq. (4), the generalized strain vectors at any point within the element can be expressed as follows:

$$\{\boldsymbol{\epsilon}_\mathbf{b}\} = [\mathbf{B_{tb}}]\{\mathbf{d}_\mathbf{t}^\mathbf{e}\} + [\mathbf{Z}_1][\mathbf{B_{rb}}]\{\mathbf{d}_\mathbf{r}^\mathbf{e}\} + [\mathbf{B_{tnb}}]\{\mathbf{d}_\mathbf{t}^\mathbf{e}\} \quad \text{and} \quad \{\boldsymbol{\epsilon}_\mathbf{s}\} = [\mathbf{B_{ts}}]\{\mathbf{d}_\mathbf{t}^\mathbf{e}\} + [\mathbf{Z}_2][\mathbf{B_{rs}}]\{\mathbf{d}_\mathbf{r}^\mathbf{e}\}. \tag{16}$$

In Eq. (16), the nodal generalized strain-displacement matrices ($[\mathbf{B_{tb}}]$, $[\mathbf{B_{rb}}]$, $[\mathbf{B_{tnb}}]$, $[\mathbf{B_{ts}}]$ and $[\mathbf{B_{rs}}]$) are given by

$$\begin{gathered}[\mathbf{B_{tb}}] = [\mathbf{L_{tb}}][\mathbf{N_t}], \quad [\mathbf{B_{rb}}] = [\mathbf{L_{rb}}][\mathbf{N_r}], \quad [\mathbf{B_{tnb}}] = [\mathbf{L_{tnb}}][\mathbf{N_t}],\\ [\mathbf{B_{ts}}] = [\mathbf{L_{ts}}][\mathbf{N_t}] \quad \text{and} \quad [\mathbf{B_{rs}}] = [\mathbf{N_r}]. \end{gathered} \tag{17}$$

Substituting Eqs. (7) and (8) into Eq. (13) and then using Eq. (16), the total potential energy $\mathbf{T_p^e}$ of a typical element augmented with the **ACLD** treatment can be expressed as:

$$\begin{aligned}\mathbf{T_p^e} = \frac{1}{2}[&\{\mathbf{d}_\mathbf{t}^\mathbf{e}\}^\mathbf{T}[\mathbf{K_{tt}^e}]\{\mathbf{d}_\mathbf{t}^\mathbf{e}\} + \{\mathbf{d}_\mathbf{t}^\mathbf{e}\}^\mathbf{T}[\mathbf{K_{tr}^e}]\{\mathbf{d}_\mathbf{r}^\mathbf{e}\} + \{\mathbf{d}_\mathbf{r}^\mathbf{e}\}^\mathbf{T}[\mathbf{K_{rt}^e}]\{\mathbf{d}_\mathbf{t}^\mathbf{e}\} + \{\mathbf{d}_\mathbf{r}^\mathbf{e}\}^\mathbf{T}[\mathbf{K_{rr}^e}]\{\mathbf{d}_\mathbf{r}^\mathbf{e}\}\\ &+ \{\mathbf{d}_\mathbf{t}^\mathbf{e}\}^\mathbf{T}[\mathbf{K_{tsv}^e}]\int_0^\mathbf{t} \mathbf{G(t-\tau)}\frac{\partial}{\partial \boldsymbol{\tau}}\{\mathbf{d}_\mathbf{t}^\mathbf{e}\}\mathbf{d}\boldsymbol{\tau} + \{\mathbf{d}_\mathbf{t}^\mathbf{e}\}^\mathbf{T}[\mathbf{K_{trsv}^e}]\int_0^\mathbf{t} \mathbf{G(t-\tau)}\frac{\partial}{\partial \boldsymbol{\tau}}\{\mathbf{d}_\mathbf{r}^\mathbf{e}\}\mathbf{d}\boldsymbol{\tau}\\ &+ \{\mathbf{d}_\mathbf{r}^\mathbf{e}\}^\mathbf{T}[\mathbf{K_{trsv}^e}]^\mathbf{T}\int_0^\mathbf{t} \mathbf{G(t-\tau)}\frac{\partial}{\partial \boldsymbol{\tau}}\{\mathbf{d}_\mathbf{t}^\mathbf{e}\} + \{\mathbf{d}_\mathbf{r}^\mathbf{e}\}^\mathbf{T}[\mathbf{K_{rrsv}^e}]\int_0^\mathbf{t} \mathbf{G(t-\tau)}\frac{\partial}{\partial \boldsymbol{\tau}}\{\mathbf{d}_\mathbf{r}^\mathbf{e}\}\mathbf{d}\boldsymbol{\tau}\\ &- 2\{\mathbf{d}_\mathbf{t}^\mathbf{e}\}^\mathbf{T}[\mathbf{F_{tpn}^e}]\mathbf{V} - 2\{\mathbf{d}_\mathbf{t}^\mathbf{e}\}^\mathbf{T}[\mathbf{F_{tp}^e}]\mathbf{V} - 2\{\mathbf{d}_\mathbf{r}^\mathbf{e}\}^\mathbf{T}[\mathbf{F_{rp}^e}]\mathbf{V} - \{\bar{\mathbf{E}}\}^\mathbf{T}[\bar{\boldsymbol{\varepsilon}}^{\mathbf{N+2}}]\{\bar{\mathbf{E}}\}\mathbf{V}^2 - 2\{\mathbf{d}_\mathbf{t}^\mathbf{e}\}^\mathbf{T}\{\mathbf{F^e}\}], \end{aligned} \tag{18}$$

in which $\bar{\mathbf{E}} = -1/\mathbf{h_p}$ and $\mathbf{V}$ is the potential difference across the thickness of the **PFRC** layer. The elemental stiffness matrices ($[\mathbf{K_{tt}^e}]$, $[\mathbf{K_{tr}^e}]$, $[\mathbf{K_{rt}^e}]$, $[\mathbf{K_{rr}^e}]$, $[\mathbf{K_{tsv}^e}]$, $[\mathbf{K_{trsv}^e}]$, $[\mathbf{K_{trsv}^e}]^\mathbf{T}$ and $[\mathbf{K_{rrsv}^e}]$), the elemental electro-elastic coupling matrices ($[\mathbf{F_{tpn}^e}]$, $[\mathbf{F_{tp}^e}]$, and $[\mathbf{F_{rp}^e}]$) and the elemental load vector $[\mathbf{F^e}]$ appearing in Eq. (18) are defined as follows:

$$[\mathbf{K_{tt}^e}] = [\mathbf{K_{tb}^e}] + [\mathbf{K_{ts}^e}] + [\mathbf{K_{tnb}^e}], \quad [\mathbf{K_{tr}^e}] = [\mathbf{K_{trb}^e}] + [\mathbf{K_{trs}^e}] + [\mathbf{K_{trbn}^e}],$$

$$[\mathbf{K_{rt}^e}] = [\mathbf{K_{trb}^e}]^\mathbf{T} + [\mathbf{K_{trs}^e}]^\mathbf{T} + \frac{1}{2}[\mathbf{K_{trbn}^e}]^\mathbf{T}, \quad [\mathbf{K_{rr}^e}] = [\mathbf{K_{rrb}^e}] + [\mathbf{K_{rrs}^e}],$$

$$[\mathbf{K_{tb}^e}] = \int_0^{\mathbf{b_e}}\int_0^{\mathbf{a_e}} [\mathbf{B_{tb}}]^\mathbf{T}[\mathbf{D_{tb}}][\mathbf{B_{tb}}]\mathbf{dxdy}, \quad [\mathbf{K_{ts}^e}] = \int_0^{\mathbf{b_e}}\int_0^{\mathbf{a_e}} [\mathbf{B_{ts}}]^\mathbf{T}[\mathbf{D_{ts}}][\mathbf{B_{ts}}]\mathbf{dxdy},$$

$$[\mathbf{K_{tnb}^e}] = \int_0^{\mathbf{b_e}}\int_0^{\mathbf{a_e}} \left(\frac{1}{2}[\mathbf{B_{tb}}]^\mathbf{T}[\mathbf{D_{tb}}][\mathbf{B}_1][\mathbf{B}_2] + [\mathbf{B}_2]^\mathbf{T}[\mathbf{B}_1]^\mathbf{T}[\mathbf{D_{tb}}][\mathbf{B_{tb}}] + \frac{1}{2}[\mathbf{B}_2]^\mathbf{T}[\mathbf{B}_1]^\mathbf{T}[\mathbf{D_{tb}}][\mathbf{B}_1][\mathbf{B}_2]\right)\mathbf{dxdy},$$

$$[\mathbf{K_{trb}^e}] = \int_0^{\mathbf{a_e}}\int_0^{\mathbf{b_e}} [\mathbf{B_{tb}}]^\mathbf{T}[\mathbf{D_{trb}}][\mathbf{B_{rb}}]\mathbf{dxdy}, \qquad [\mathbf{K_{trs}^e}] = \int_0^{\mathbf{a_e}}\int_0^{\mathbf{b_e}} [\mathbf{B_{rs}}]^\mathbf{T}[\mathbf{D_{trs}}][\mathbf{B_{ts}}]\mathbf{dxdy},$$

$$[\mathbf{K_{trbn}^e}] = \int_0^{\mathbf{a_e}}\int_0^{\mathbf{b_e}} [\mathbf{B}_2]^\mathbf{T}[\mathbf{B}_1]^\mathbf{T}[\mathbf{D_{trb}}][\mathbf{B_{rb}}]\mathbf{dxdy}, \quad [\mathbf{K_{rrb}^e}] = \int_0^{\mathbf{a_e}}\int_0^{\mathbf{b_e}} [\mathbf{B_{rb}}]^\mathbf{T}[\mathbf{D_{rrb}}][\mathbf{B_{rb}}]\mathbf{dxdy},$$

$$[\mathbf{K^e_{rrs}}] = \int_0^{\mathbf{a_e}}\int_0^{\mathbf{b_e}} [\mathbf{B_{rs}}]^{\mathbf{T}}[\mathbf{D_{rrs}}][\mathbf{B_{rs}}]\mathbf{dxdy}, \quad [\mathbf{K^e_{tsv}}] = \mathbf{h_v}\int_0^{\mathbf{b_e}}\int_0^{\mathbf{a_e}} [\mathbf{B_{ts}}]^{\mathbf{T}}[\mathbf{B_{ts}}]\mathbf{dxdy},$$

$$[\mathbf{K^e_{trsv}}] = \mathbf{h_v}\int_0^{\mathbf{b_e}}\int_0^{\mathbf{a_e}} [\mathbf{B_{ts}}]^{\mathbf{T}}[\mathbf{Z_2}][\mathbf{B_{rs}}]\mathbf{dxdy}, \quad [\mathbf{K^e_{rrsv}}] = \mathbf{h_v}\int_0^{\mathbf{b_e}}\int_0^{\mathbf{a_e}} [\mathbf{B_{rs}}]^{\mathbf{T}}[\mathbf{Z_2}]^{\mathbf{T}}[\mathbf{Z_2}][\mathbf{B_{rs}}]\mathbf{dxdy},$$

$$[\mathbf{F^e_{tpn}}] = \int_0^{\mathbf{b_e}}\int_0^{\mathbf{a_e}} [\mathbf{B_2}]^{\mathbf{T}}[\mathbf{B_1}]^{\mathbf{T}}\{\mathbf{F_{tb}}\}_{\mathbf{p}}\mathbf{dxdy}, \quad [\mathbf{F^e_{tp}}] = \int_0^{\mathbf{b_e}}\int_0^{\mathbf{a_e}} ([\mathbf{B_{tb}}]^{\mathbf{T}}\{\mathbf{F_{tb}}\}_{\mathbf{p}}\mathbf{dxdy},$$

$$[\mathbf{F^e_{rp}}] = \int_0^{\mathbf{b_e}}\int_0^{\mathbf{a_e}} ([\mathbf{B_{rb}}]^{\mathbf{T}}\{\mathbf{F_{rb}}\}_{\mathbf{p}}\mathbf{dxdy} \quad \text{and} \quad [\mathbf{F^e}] = \int_0^{\mathbf{b_e}}\int_0^{\mathbf{a_e}} [\mathbf{N_t}]^{\mathbf{T}}\{\mathbf{f}\}\mathbf{dxdy},$$

where $\mathbf{a_e}$ and $\mathbf{b_e}$ are the length and width of the element under consideration, and the various rigidity matrices originated in the above elemental matrices are:

$$[\mathbf{D_{tb}}] = \sum_{\mathbf{k=1}}^{\mathbf{N}} \int_{\mathbf{h_k}}^{\mathbf{h_{k+1}}} [\bar{\mathbf{C}}^{\mathbf{k}}_{\mathbf{b}}]\mathbf{dz} + \int_{\mathbf{h_{N+2}}}^{\mathbf{h_{N+3}}} [\bar{\mathbf{C}}^{\mathbf{N+2}}_{\mathbf{b}}]\mathbf{dz}, \quad [\mathbf{D_{trb}}] = \sum_{\mathbf{k=1}}^{\mathbf{N}} \int_{\mathbf{h_k}}^{\mathbf{h_{k+1}}} [\bar{\mathbf{C}}^{\mathbf{k}}_{\mathbf{b}}][\mathbf{Z_1}]\mathbf{dz} + \int_{\mathbf{h_{N+2}}}^{\mathbf{h_{N+3}}} [\bar{\mathbf{C}}^{\mathbf{N+2}}_{\mathbf{b}}][\mathbf{Z_1}]\mathbf{dz},$$

$$[\mathbf{D_{rrb}}] = \sum_{\mathbf{k=1}}^{\mathbf{N}} \int_{\mathbf{h_k}}^{\mathbf{h_{k+1}}} [\mathbf{Z_1}]^{\mathbf{T}}[\bar{\mathbf{C}}^{\mathbf{k}}_{\mathbf{b}}][\mathbf{Z_1}]\mathbf{dz} + \int_{\mathbf{h_{N+2}}}^{\mathbf{h_{N+3}}} [\mathbf{Z_1}]^{\mathbf{T}}[\bar{\mathbf{C}}^{\mathbf{N+2}}_{\mathbf{b}}][\mathbf{Z_1}]\mathbf{dz},$$

$$[\mathbf{D_{ts}}] = \sum_{\mathbf{k=1}}^{\mathbf{N}} \int_{\mathbf{h_k}}^{\mathbf{h_{k+1}}} [\bar{\mathbf{C}}^{\mathbf{k}}_{\mathbf{s}}]\mathbf{dz} + \int_{\mathbf{h_{N+2}}}^{\mathbf{h_{N+3}}} [\bar{\mathbf{C}}^{\mathbf{N+2}}_{\mathbf{s}}]\mathbf{dz}, \quad [\mathbf{D_{trs}}] = \sum_{\mathbf{k=1}}^{\mathbf{N}} \int_{\mathbf{h_k}}^{\mathbf{h_{k+1}}} [\bar{\mathbf{C}}^{\mathbf{k}}_{\mathbf{s}}][\mathbf{Z_2}]\mathbf{dz} + \int_{\mathbf{h_{N+2}}}^{\mathbf{h_{N+3}}} [\bar{\mathbf{C}}^{\mathbf{N+2}}_{\mathbf{s}}][\mathbf{Z_2}]\mathbf{dz},$$

$$[\mathbf{D_{rrs}}] = \sum_{\mathbf{k=1}}^{\mathbf{N}} \int_{\mathbf{h_k}}^{\mathbf{h_{k+1}}} [\mathbf{Z_2}]^{\mathbf{T}}[\bar{\mathbf{C}}^{\mathbf{k}}_{\mathbf{s}}][\mathbf{Z_2}]\mathbf{dz} + \int_{\mathbf{h_{N+2}}}^{\mathbf{h_{N+3}}} [\mathbf{Z_2}]^{\mathbf{T}}[\bar{\mathbf{C}}^{\mathbf{N+2}}_{\mathbf{b}}][\mathbf{Z_2}]\mathbf{dz},$$

$$\{\mathbf{F_{tb}}\}_{\mathbf{p}} = \int_{\mathbf{h_{N+2}}}^{\mathbf{h_{N+3}}} [\bar{\mathbf{e}}^{\mathbf{N+2}}_{\mathbf{b}}]\{\bar{\mathbf{E}}\}\mathbf{dz}, \quad \{\mathbf{F_{rb}}\}_{\mathbf{p}} = \int_{\mathbf{h_{N+2}}}^{\mathbf{h_{N+3}}} [\mathbf{Z_1}]^{\mathbf{T}}[\bar{\mathbf{e}}^{\mathbf{N+2}}_{\mathbf{b}}]\{\bar{\mathbf{E}}\}\mathbf{dz}.$$

Substituting Eq. (14) into Eq. (12), the expression for the kinetic energy $\mathbf{T^e_k}$ of the element can be obtained as

$$\mathbf{T^e_k} = \frac{1}{2}\{\dot{\mathbf{d}}^{\mathbf{e}}_{\mathbf{t}}\}^{\mathbf{T}}[\mathbf{M^e}]\{\mathbf{d^e_t}\}, \tag{19}$$

in which $[\mathbf{M^e}] = \int_0^{\mathbf{b_e}}\int_0^{\mathbf{a_e}} \bar{\mathbf{m}}\{\mathbf{N_t}\}^{\mathbf{T}}[\mathbf{N_t}]\mathbf{dxdy}$ and $\bar{\mathbf{m}} = \sum_{\mathbf{k=1}}^{\mathbf{N}} \boldsymbol{\rho}^{\mathbf{k}}(\mathbf{h_{k+1}} - \mathbf{h_k}) + \boldsymbol{\rho}^{\mathbf{N+1}}\mathbf{h_v} + \boldsymbol{\rho}^{\mathbf{N+2}}\mathbf{h_p}$.

The rotary inertia of the overall plate has been neglected to estimate the total kinetic energy of the element because the substrate plates considered here are very thin. Now, applying Hamilton's principle [20], the following governing equations of motion of an element are obtained:

$$[\mathbf{M^e}]\{\ddot{\mathbf{d}}^{\mathbf{e}}_{\mathbf{t}}\} + [\mathbf{K^e_{tt}}]\{\mathbf{d^e_t}\} + [\mathbf{K^e_{tr}}]\{\mathbf{d^e_r}\} + [\mathbf{K^e_{tsv}}]\int_0^{\mathbf{t}} \mathbf{G}(\mathbf{t}-\boldsymbol{\tau})\frac{\boldsymbol{\partial}}{\boldsymbol{\partial\tau}}\{\mathbf{d^e_t}\}\mathbf{d}\boldsymbol{\tau}$$

$$+ [\mathbf{K^e_{trsv}}]\int_0^{\mathbf{t}} \mathbf{G}(\mathbf{t}-\boldsymbol{\tau})\frac{\boldsymbol{\partial}}{\boldsymbol{\partial\tau}}\{\mathbf{d^e_r}\}\boldsymbol{\partial\tau} = \{\mathbf{F^e}\} + ([\mathbf{F^e_{tpn}}] + [\mathbf{F^e_{tp}}])\mathbf{V}, \tag{20}$$

$$[\mathbf{K}^{\mathbf{e}}_{\mathbf{rt}}]\{\mathbf{d}^{\mathbf{e}}_{\mathbf{t}}\} + [\mathbf{K}^{\mathbf{e}}_{\mathbf{rr}}]\{\mathbf{d}^{\mathbf{e}}_{\mathbf{r}}\} + [\mathbf{K}^{\mathbf{e}}_{\mathbf{trsv}}]^{\mathbf{T}} \int_0^{\mathbf{t}} \mathbf{G}(\mathbf{t}-\boldsymbol{\tau}) \frac{\boldsymbol{\partial}}{\boldsymbol{\partial \tau}} \{\mathbf{d}^{\mathbf{e}}_{\mathbf{t}}\} \mathbf{d}\boldsymbol{\tau}$$

$$+ [\mathbf{K}^{\mathbf{e}}_{\mathbf{rrsv}}] \int_0^{\mathbf{t}} \mathbf{G}(\mathbf{t}-\boldsymbol{\tau}) \frac{\boldsymbol{\partial}}{\boldsymbol{\partial \tau}} \{\mathbf{d}^{\mathbf{e}}_{\mathbf{r}}\} \mathbf{d}\boldsymbol{\tau} = \{\mathbf{F}^{\mathbf{e}}_{\mathbf{rp}}\}\mathbf{V}. \tag{21}$$

It should be noted here that for an element without integration with the **ACLD** patch, the matrices $[\mathbf{F}^{\mathbf{e}}_{\mathbf{tpn}}]$, $[\mathbf{F}^{\mathbf{e}}_{\mathbf{tp}}]$ and $[\mathbf{F}^{\mathbf{e}}_{\mathbf{rp}}]$ turn out to be the null matrices.

The elemental governing equations are assembled into the global space to obtain the global equations of equilibrium as follows:

$$[\mathbf{M}]\{\ddot{\mathbf{X}}_{\mathbf{t}}\} + [\mathbf{K}_{\mathbf{tt}}]\{\mathbf{X}_{\mathbf{t}}\} + [\mathbf{K}_{\mathbf{tr}}]\{\mathbf{X}_{\mathbf{r}}\} + [\mathbf{K}_{\mathbf{tsv}}] \int_{\mathbf{0}}^{\mathbf{t}} \mathbf{G}(\mathbf{t}-\boldsymbol{\tau}) \frac{\boldsymbol{\partial}}{\boldsymbol{\partial \tau}} \{\mathbf{X}_{\mathbf{t}}\} \boldsymbol{\partial \tau}$$

$$+ [\mathbf{K}_{\mathbf{trsv}}] \int_0^{\mathbf{t}} \mathbf{G}(\mathbf{t}-\boldsymbol{\tau}) \frac{\boldsymbol{\partial}}{\boldsymbol{\partial \tau}} \{\mathbf{X}_{\mathbf{r}}\} \mathbf{d}\boldsymbol{\tau} = \{\mathbf{F}\} + (\{\mathbf{F}_{\mathbf{tpn}}\} + \{\mathbf{F}_{\mathbf{tp}}\})\mathbf{V}, \tag{22}$$

$$[\mathbf{K}_{\mathbf{rt}}]\{\mathbf{X}_{\mathbf{t}}\} + [\mathbf{K}_{\mathbf{rr}}]\{\mathbf{X}_{\mathbf{r}}\} + [\mathbf{K}_{\mathbf{trsv}}]^{\mathbf{T}} \int_{\mathbf{0}}^{\mathbf{t}} \mathbf{G}(\mathbf{t}-\boldsymbol{\tau}) \frac{\boldsymbol{\partial}}{\boldsymbol{\partial \tau}} \{\mathbf{X}_{\mathbf{t}}\} \mathbf{d}\boldsymbol{\tau}$$

$$+ [\mathbf{K}_{\mathbf{rrsv}}] \int_0^{\mathbf{t}} \mathbf{G}(\mathbf{t}-\boldsymbol{\tau}) \frac{\boldsymbol{\partial}}{\boldsymbol{\partial \tau}} \{\mathbf{X}_{\mathbf{r}}\} \mathbf{d}\boldsymbol{\tau} = \{\mathbf{F}_{\mathbf{rp}}\}\mathbf{V}, \tag{23}$$

where $[\mathbf{M}]$ is the global mass matrix; $[\mathbf{K}_{\mathbf{tt}}]$, $[\mathbf{K}_{\mathbf{tr}}]$, $[\mathbf{K}_{\mathbf{rt}}]$, $[\mathbf{K}_{\mathbf{rr}}]$, $[\mathbf{K}_{\mathbf{tsv}}]$, $[\mathbf{K}_{\mathbf{trsv}}]$ and $[\mathbf{K}_{\mathbf{rrsv}}]$ are the global stiffness matrices; $[\mathbf{F}_{\mathbf{tpn}}]$, $[\mathbf{F}_{\mathbf{tp}}]$ and $[\mathbf{F}_{\mathbf{rp}}]$ are the global electro-elastic coupling matrices; $\{\mathbf{X}_{\mathbf{t}}\}$ and $\{\mathbf{X}_{\mathbf{r}}\}$ are the global nodal generalized displacement vectors; $\{\mathbf{F}\}$ is the global nodal mechanical force vector; and $\mathbf{V}$ is the voltage applied to each patch.

In the Laplace domain, the function $\mathbf{s}\tilde{\mathbf{G}}(\mathbf{s})$ is referred to as the material modulus function with $\tilde{\mathbf{G}}(\mathbf{s})$ being the Laplace transform of the material relaxation function $\mathbf{G}(\mathbf{t})$ of the viscoelastic material. According to the Golla–Hughes–McTavish **(GHM)** method for modeling the viscoelastic material in time domain, the material modulus function can be represented by a series of mini-oscillator terms as follows [37]:

$$\mathbf{s}\tilde{\mathbf{G}}(\mathbf{s}) = \mathbf{G}^{\infty}\left[1 + \sum_{\mathbf{k}=\mathbf{1}}^{\mathbf{n}} \boldsymbol{\alpha}_{\mathbf{k}} \frac{\mathbf{s}^2 + 2\hat{\boldsymbol{\xi}}_{\mathbf{k}}\hat{\boldsymbol{\omega}}_{\mathbf{k}}\mathbf{s}}{\mathbf{s}^2 + 2\hat{\boldsymbol{\xi}}\hat{\boldsymbol{\omega}}_{\mathbf{k}}\mathbf{s} + \hat{\boldsymbol{\omega}}_{\mathbf{k}}^2}\right], \tag{24}$$

where $\mathbf{G}^{\infty}$ corresponds to the equilibrium value of the modulus, that is, the final value of the relaxation $\mathbf{G}(\mathbf{t})$. Each mini-oscillator term is a second-order rational function involving three positive constants $\boldsymbol{\alpha}_{\mathbf{k}}$, $\hat{\boldsymbol{\omega}}_{\mathbf{k}}$ and $\hat{\boldsymbol{\xi}}_{\mathbf{k}}$. These constants govern the shape of the modulus function in the complex $\mathbf{s}$ domain. Now considering a **GHM** material modulus function with one mini-oscillator term [37], that is,

$$\mathbf{s}\tilde{\mathbf{G}}(\mathbf{s}) = \mathbf{G}^{\infty}\left[1 + \boldsymbol{\alpha}\frac{\mathbf{s}^2 + 2\hat{\boldsymbol{\xi}}\hat{\boldsymbol{\omega}}\mathbf{s}}{\mathbf{s}^2 + 2\hat{\boldsymbol{\xi}}\hat{\boldsymbol{\omega}}\mathbf{s} + \hat{\boldsymbol{\omega}}^2}\right], \tag{25}$$

the auxiliary dissipation coordinates $\{\mathbf{Z}_{\mathbf{t}}\}$, $\{\mathbf{Z}_{\mathbf{r}}\}$ are introduced as follows:

$$\{\tilde{\mathbf{Z}}_{\mathbf{t}}(\mathbf{s})\} = \frac{\hat{\boldsymbol{\omega}}^2}{\mathbf{s}^2 + 2\hat{\boldsymbol{\xi}}\hat{\boldsymbol{\omega}}\mathbf{s} + \hat{\boldsymbol{\omega}}^2}\{\tilde{\mathbf{X}}_{\mathbf{t}}\} \quad \text{and} \quad \{\tilde{\mathbf{Z}}_{\mathbf{r}}(\mathbf{s})\} = \frac{\hat{\boldsymbol{\omega}}^2}{\mathbf{s}^2 + 2\hat{\boldsymbol{\xi}}\hat{\boldsymbol{\omega}}\mathbf{s} + \hat{\boldsymbol{\omega}}^2}\{\tilde{\mathbf{X}}_{\mathbf{r}}\}, \tag{26}$$

where $\{\tilde{\mathbf{Z}}(\mathbf{s})\}$ and $\{\tilde{\mathbf{Z}}_{\mathbf{r}}(\mathbf{s})\}$ are the Laplace transforms of $\{\mathbf{Z}_{\mathbf{t}}\}$ and $\{\mathbf{Z}_{\mathbf{r}}\}$, respectively.

Taking the inverse Laplace transform of Eq. (26), the time-domain representation of the auxiliary dissipation coordinates can be written as

$$\{\ddot{\mathbf{Z}}_\mathbf{t}\} + 2\hat{\xi}\hat{\omega}\{\dot{\mathbf{Z}}_\mathbf{t}\} + \hat{\omega}^2\{\mathbf{Z}_\mathbf{t}\} - \hat{\omega}^2\{\mathbf{X}_\mathbf{t}\} = 0, \tag{27}$$

$$\{\ddot{\mathbf{Z}}_\mathbf{r}\} + 2\hat{\xi}\hat{\omega}\{\dot{\mathbf{Z}}_\mathbf{r}\} + \hat{\omega}^2\{\mathbf{Z}_\mathbf{r}\} - \hat{\omega}^2\{\mathbf{X}_\mathbf{r}\} = 0. \tag{28}$$

Making use of Eqs. (25) and (26) in the Laplace transform of Eqs. (22) and (23) and subsequently taking the inverse Laplace transform of the resulting equations, the following global equations of motion are obtained:

$$\begin{aligned}&[\mathbf{M}]\{\ddot{\mathbf{X}}_\mathbf{t}\} + [\bar{\mathbf{K}}_\mathbf{tt}]\{\mathbf{X}_\mathbf{t}\} + [\bar{\mathbf{K}}_\mathbf{tr}]\{\mathbf{X}_\mathbf{r}\} - [\mathbf{K}_\mathbf{tsv}]\mathbf{G}^\infty\boldsymbol{\alpha}\{\mathbf{Z}\}\\ &\quad - [\mathbf{K}_\mathbf{trsv}]\mathbf{G}^\infty\boldsymbol{\alpha}\{\mathbf{Z}_\mathbf{r}\} = \{\mathbf{F}\} + (\{\mathbf{F}_\mathbf{tp}\} + \{\mathbf{F}_\mathbf{tpn}\})\mathbf{V},\end{aligned} \tag{29}$$

$$[\bar{\mathbf{K}}_\mathbf{rt}]\{\mathbf{X}_\mathbf{t}\} + [\bar{\mathbf{K}}_\mathbf{rr}]\{\mathbf{X}_\mathbf{r}\} - [\mathbf{K}_\mathbf{trsv}]^\mathbf{T}\mathbf{G}^\infty\boldsymbol{\alpha}\{\mathbf{Z}\} - [\mathbf{K}_\mathbf{rrsv}]\mathbf{G}^\infty\boldsymbol{\alpha}\{\mathbf{Z}_\mathbf{r}\} = \{\tilde{\mathbf{F}}_\mathbf{rp}\}\mathbf{V}, \tag{30}$$

in which

$$[\bar{\mathbf{K}}_\mathbf{tt}] = [\mathbf{K}_\mathbf{tt}] + [\mathbf{K}_\mathbf{tsv}]\mathbf{G}^\infty(1+\boldsymbol{\alpha}),\ [\bar{\mathbf{K}}_\mathbf{tr}] = [\mathbf{K}_\mathbf{tr}] + [\mathbf{K}_\mathbf{trsv}]\mathbf{G}^\infty(1+\boldsymbol{\alpha}),$$
$$[\bar{\mathbf{K}}_\mathbf{rr}] = [\mathbf{K}_\mathbf{rr}] + [\mathbf{K}_\mathbf{rrsv}]\mathbf{G}^\infty(1+\boldsymbol{\alpha}),\ [\bar{\mathbf{K}}_\mathbf{rt}] = [\mathbf{K}_\mathbf{rt}] + [\mathbf{K}_\mathbf{trsv}]^\mathbf{T}\mathbf{G}^\infty(1+\boldsymbol{\alpha}).$$

Now, the global rotational degrees of freedom can be condensed from Eqs. (28)–(30) to obtain the following global open-loop equations of motion in terms of the global translational degrees of freedom $\{\mathbf{X}_\mathbf{t}\}$and the dissipation coordinates $\{\mathbf{Z}_\mathbf{t}\}$, $\{\mathbf{Z}_\mathbf{r}\}$ as follows:

$$[\mathbf{M}]\{\ddot{\mathbf{X}}_\mathbf{t}\} + [\mathbf{K}_\mathbf{x}]\{\mathbf{X}_\mathbf{t}\} + [\mathbf{K}_\mathbf{z}]\{\mathbf{Z}_\mathbf{t}\} + [\mathbf{K}_\mathbf{zr}]\{\mathbf{Z}_\mathbf{r}\} = \{\mathbf{F}\} + \{\mathbf{F}_\mathbf{p}\}\mathbf{V}, \tag{31}$$

$$\{\ddot{\mathbf{Z}}_\mathbf{r}\} + 2\hat{\xi}\hat{\omega}\{\dot{\mathbf{Z}}_\mathbf{r}\} + \hat{\omega}^2[\mathbf{K}_1]\{\mathbf{X}_\mathbf{t}\} - \hat{\omega}^2[\mathbf{K}_2]\{\mathbf{Z}\} + \hat{\omega}^2[\mathbf{K}_3]\{\mathbf{Z}_\mathbf{r}\} = \{\mathbf{F}_\mathbf{pz}\}\mathbf{V} \tag{32}$$

where

$$\begin{aligned}&[\mathbf{K}_\mathbf{x}] = [\bar{\mathbf{K}}_\mathbf{tt}] - [\bar{\mathbf{K}}_\mathbf{tr}][\bar{\mathbf{K}}_\mathbf{rr}]^{-1}[\bar{\mathbf{K}}_\mathbf{rt}],\quad [\mathbf{K}_\mathbf{z}] = [\bar{\mathbf{K}}_\mathbf{tr}][\bar{\mathbf{K}}_\mathbf{rr}]^{-1}[\mathbf{K}_\mathbf{trsv}]^\mathbf{T}\mathbf{G}^\infty\boldsymbol{\alpha} - [\mathbf{K}_\mathbf{tsv}]\mathbf{G}^\infty\boldsymbol{\alpha},\\ &[\mathbf{K}_\mathbf{zr}] = [\bar{\mathbf{K}}_\mathbf{tr}][\bar{\mathbf{K}}_\mathbf{rr}]^{-1}[\mathbf{K}_\mathbf{rrsv}]\mathbf{G}^\infty\boldsymbol{\alpha} - [\mathbf{K}_\mathbf{trsv}]\mathbf{G}^\infty\boldsymbol{\alpha},\quad \{\mathbf{F}_\mathbf{P}\} = \{\mathbf{F}_\mathbf{tp}\} + \{\mathbf{F}_\mathbf{tpn}\} + [\bar{\mathbf{K}}_\mathbf{tr}][\bar{\mathbf{K}}_\mathbf{rr}]^{-1}\{\mathbf{F}_\mathbf{rp}\},\\ &[\mathbf{K}_1] = [\bar{\mathbf{K}}_\mathbf{rr}]^{-1}[\mathbf{K}_\mathbf{rt}],\quad [\mathbf{K}_2] = [\bar{\mathbf{K}}_\mathbf{rr}]^{-1}[\mathbf{K}_\mathbf{trsv}]^\mathbf{T}\mathbf{G}^\infty\boldsymbol{\alpha},\quad [\mathbf{K}_3] = \mathbf{I}_\mathbf{zr} - [\bar{\mathbf{K}}_\mathbf{rr}]^{-1}[\mathbf{K}_\mathbf{rrsv}]\mathbf{G}^\infty\boldsymbol{\alpha},\\ &\{\mathbf{F}_\mathbf{pz}\} = \hat{\omega}^2[\mathbf{K}_\mathbf{rr}]^{-1}\{\mathbf{F}_\mathbf{rp}\}.\end{aligned}$$

Now, the global equations of motion given by Eqs. (27), (31) and (32) can be combined to form a single set of equations governing the coupled electro-elastic open-loop behavior of the laminated composite plate integrated with the patches of ACLD treatment as follows:

$$[\mathbf{M}^*]\{\ddot{\mathbf{X}}\} + [\mathbf{C}^*]\{\dot{\mathbf{X}}\} + [\mathbf{K}^*]\{\mathbf{X}\} = \{\mathbf{F}^*\} + \{\mathbf{F}^*_\mathbf{p}\}\mathbf{V}, \tag{33}$$

in which

$$[\mathbf{M}^*] = \begin{bmatrix}[\mathbf{M}] & 0 & 0\\ 0 & \mathbf{I}_\mathbf{z} & 0\\ 0 & 0 & \mathbf{I}_\mathbf{zr}\end{bmatrix},\quad [\mathbf{K}^*] = \begin{bmatrix}[\mathbf{K}_\mathbf{x}] & [\mathbf{K}_\mathbf{z}] & [\mathbf{K}_\mathbf{zr}]\\ -\hat{\omega}^2\mathbf{I}_\mathbf{z} & \hat{\omega}^2\mathbf{I}_\mathbf{z} & 0\\ \hat{\omega}^2[\mathbf{K}_1] & -\hat{\omega}^2[\mathbf{K}_2] & \hat{\omega}^2[\mathbf{K}_3]\end{bmatrix},\quad [\mathbf{C}^*] = \begin{bmatrix}0 & 0 & 0\\ 0 & 2\hat{\xi}\hat{\omega} & 0\\ 0 & 0 & 2\hat{\xi}\hat{\omega}\end{bmatrix},$$

$$\{\mathbf{F}^*\} = \begin{Bmatrix}\{\tilde{\mathbf{F}}\}\\ 0\\ 0\end{Bmatrix},\quad \{\mathbf{F}^*_\mathbf{p}\} = \begin{Bmatrix}\{\mathbf{F}_\mathbf{p}\}\\ 0\\ \{\mathbf{F}_\mathbf{pz}\}\end{Bmatrix}\ \text{and}\ \{\mathbf{X}\} = \begin{Bmatrix}\{\mathbf{X}_\mathbf{t}\}\\ \{\mathbf{Z}_\mathbf{t}\}\\ \{\mathbf{Z}_\mathbf{r}\}\end{Bmatrix},$$

where $\mathbf{I}_\mathbf{z}$ and $\mathbf{I}_\mathbf{zr}$ are identity matrices of appropriate sizes associated with the dissipation coordinates $\{\mathbf{Z}_\mathbf{t}\}$ and $\{\mathbf{Z}_\mathbf{r}\}$, respectively.

3 Closed-loop model

In order to apply the control voltage for activating the patches of the **ACLD** treatment, a simple velocity feedback control law has been employed. According to this law, the control voltage for each patch can be expressed in terms of the derivatives of the global nodal degrees of freedom as follows:

$$\mathbf{V^j} = -\mathbf{K_d^j}\dot{\mathbf{w}} = -\mathbf{K_d^j}[\mathbf{U^j}]\{\dot{\mathbf{X}}\}, \tag{34}$$

in which $\mathbf{K_d^j}$ is the control gain for the **j**th patch and $[\mathbf{U^j}]$ is a unit vector defining the location of sensing the velocity signal that will be fed back to this patch. Finally, substituting Eq. (34) into Eq. (33), the equations of motion governing the closed-loop dynamics of the substrate plates activated by the patches of **ACLD** treatments can be obtained as follows:

$$[\mathbf{M^*}]\{\ddot{\mathbf{X}}\} + [\mathbf{C_d^*}]\{\dot{\mathbf{X}}\} + [\mathbf{K^*}]\{\mathbf{X}\} = \{\mathbf{F^*}\}, \tag{35}$$

where $[\mathbf{C_d^*}] = [\mathbf{C^*}] + \sum_{\mathbf{j=1}}^{\mathbf{m}} \mathbf{K_d^j}\{\mathbf{F_p^*}\}[\mathbf{U^j}]$ is an active damping matrix.

4 Numerical results

In this section, the numerical results are evaluated using the finite element model derived in the previous section for assessing the performance of the **ACLD** patches on controlling the geometrically nonlinear vibrations of laminated composite shallow shells. Symmetric/antisymmetric cross-ply and antisymmetric angle-ply thin circular cylindrical panels having the square plan form ($\mathbf{a} \times \mathbf{a}$) and integrated with two rectangular patches of **ACLD** treatment (Fig. 1) are considered for evaluating the numerical results. The results are presented for various shallowness angles ($\boldsymbol{\phi}$) of the thin cylindrical panel. The material properties considered for the orthotropic layers of the substrate panel are considered as follows:

$$\begin{gathered}\mathbf{E_L} = 172.9\,\text{GPa}, \quad \mathbf{E_L}/\mathbf{E_T} = 25, \quad \mathbf{G_{LT}} = 0.5\mathbf{E_T}, \quad \mathbf{G_{TT}} = 0.2\mathbf{E_T}, \\ \boldsymbol{\nu}_{\mathbf{LT}} = \boldsymbol{\nu}_{\mathbf{TT}} = 0.25, \boldsymbol{\rho} = 1,600\,\text{kg/m}^3,\end{gathered} \tag{36}$$

in which the symbols have their usual meaning. The piezoelectric fibers and the matrix of the **PFRC** patches are made of **PZT5H** and epoxy, respectively. The effective elastic and piezoelectric coefficients of the **PFRC** with 40 % fiber volume fraction are obtained by using the micro-mechanics model derived by Mallik and Ray [27] and are given by

$$\begin{gathered}\mathbf{C}_{11} = 32.6\,\text{GPa}, \quad \mathbf{C}_{12} = 4.3\,\text{GPa}, \quad \mathbf{C}_{22} = 7.2\,\text{GPa}, \quad \mathbf{C}_{44} = 1.05\,\text{GPa}, \quad \mathbf{C}_{55} = \mathbf{C}_{66} = 1.29\,\text{GPa}, \\ \boldsymbol{\rho_p} = 3640\,\text{kg/m}^3, \mathbf{e}_{31} = -6.76\,\text{C/m}^2, \mathbf{e}_{32} = -0.076\,\text{C/m}^2.\end{gathered} \tag{37}$$

The thicknesses of the **PFRC** patch, the viscoelastic patch and the laminated panel are considered as 250 μm, 50.8 μm and 3 mm, respectively. Also, unless otherwise mentioned, the values of the axial length (**a**), the shallowness angle ($\boldsymbol{\phi}$) of the panel and piezoelectric fiber orientation angle ($\boldsymbol{\psi}$) in the **PFRC** patches are considered as 0.5 m, 20° and 0°, respectively. Also, the thicknesses of the orthotropic layers of the substrate panel are equal. The mechanical load **p** acting upward is assumed to be uniformly distributed. Considering a single-term **GHM** expression, the values of $\boldsymbol{\alpha}$, $\hat{\boldsymbol{\omega}}$ and $\hat{\boldsymbol{\xi}}$ are taken as 8.3228×10^3 and 20, respectively [38]. The shear modulus ($\mathbf{G}^{\infty}$) and the density of the viscoelastic material ($\boldsymbol{\rho_v}$) are taken as 3.9987×10^5Pa and 1,104 kg/m^3, respectively. The simply supported boundary conditions at the edges of the overall panels considered for evaluating the numerical results are given by

$$\mathbf{v}_0 = \mathbf{w} = \boldsymbol{\theta_y} = \boldsymbol{\phi_y} = \boldsymbol{\gamma_y} = 0 \quad \text{at } \mathbf{x} = 0, \mathbf{a} \quad \text{and} \quad \mathbf{u}_0 = \mathbf{w} = \boldsymbol{\theta_x} = \boldsymbol{\phi_x} = \boldsymbol{\gamma_x} = 0 \quad \text{at } \mathbf{y} = 0, \mathbf{s}.$$

Following the approach by Lim et al. [38], first the validity of the present **GHM** method for modeling the **ACLD** treatment is checked. For this, a symmetric cross-ply (0°/90°/0°) cylindrical composite panel integrated with the **ACLD** patches as shown in Fig. 1 is considered. The linear frequency responses for the transverse displacement of the panel are evaluated when the viscoelastic material is modeled by the **GHM** method and the conventional complex modulus approach, separately. A time-harmonic load of −1 N is considered to excite the first few modes of the substrate. Figure 3 illustrates the frequency functions computed by

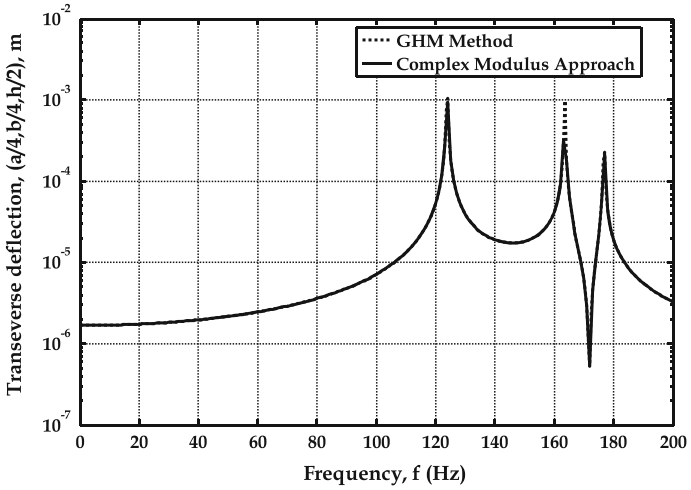

Fig. 3 Comparison of GHM result with complex stiffness solution for a simply supported antisymmetric (0°/90°/0°) substrate Panel ($\phi = 20°$), subjected to point load (-1 **N**) at (**a/4, b/4, h/2**)

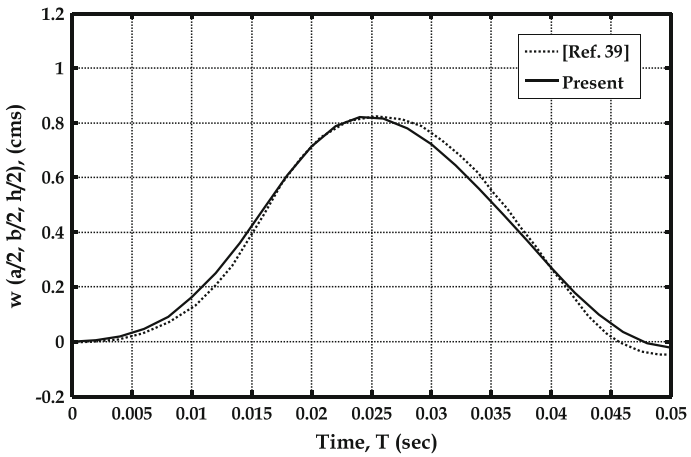

Fig. 4 Comparison of nonlinear dynamic response of simply supported (SS2) antisymmetric angle-ply (45°/ − 45°) plate with identical smart composite plate with negligible thickness of ACLD patches

both the **GHM** method and the conventional complex modulus approach for this simply supported symmetric cross-ply substrate panel of square plan form. It may be clearly observed from Fig. 3 that the frequency response curves obtained by the two approaches are almost indistinguishable. Thus the present method of modeling the viscoelastic material by the **GHM** method accurately predicts the damping characteristics of the overall panel. In order to verify the numerical integration scheme for computing the nonlinear response in time domain, the thickness of the patches of the **ACLD** treatment is considered to be negligibly small and the transient response for the center deflection of the plate computed by the present model is compared with the existing results [39] for an identical composite plate without integrated with the **ACLD** patches. It can be observed from Fig. 4 that the results obtained by the present scheme closely agree with the existing results.

The open-loop and closed-loop behavior of the substrate panels are studied by the time responses for the transverse deflection at the center of the panel ($\mathbf{a}/2,\ \mathbf{a}/2,\ \mathbf{h}/2$) on the top of the substrates. A uniformly distributed transverse pulse load is applied to set the overall panel into motion. The nondimensional mechanical load ($\mathbf{Q} = \mathbf{pa}^4/(\mathbf{E_T h}^4)$) is applied such that the overall panel undergoes nonlinear deformations. The control voltage applied to **ACLD** patch is negatively proportional to the velocity at a point ($\mathbf{a}/2,\ \mathbf{a}/2,\ \mathbf{h}/2$). The control gain is chosen arbitrarily such that the nonlinear vibrations are under control. Figure 5 illustrates the nonlinear transient responses for a simply supported symmetric cross-ply (0°/90°/0°) substrate panel with shallowness angle $\phi = 20°$. Displayed in this figure are the responses when the patches are passive (gain = 0)

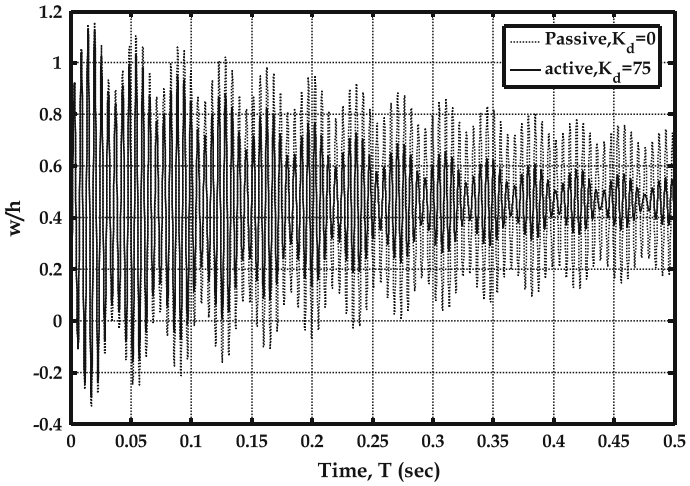

Fig. 5 Nonlinear dynamic responses of a simply supported symmetric cross-ply (0°/90°/0°) panel undergoing ACLD ($\mathbf{Q} = 750$, $\boldsymbol{\phi} = 20°$)

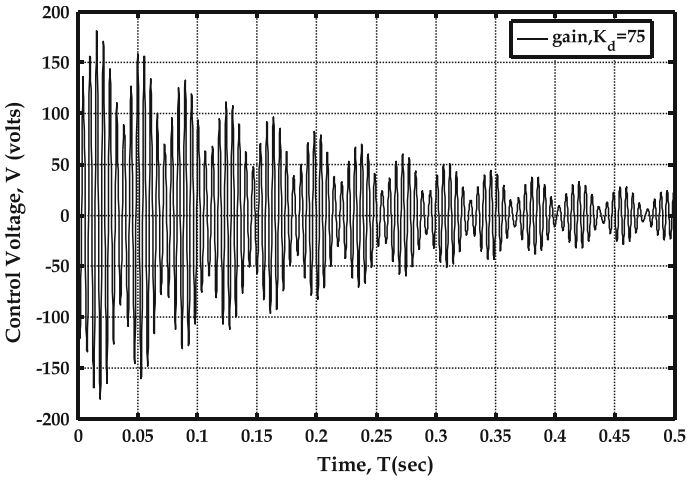

Fig. 6 Control voltages required for the ACLD of nonlinear transient vibrations of a simply supported symmetric (0°/90°/0°) panel ($\mathbf{Q} = 750$, $\boldsymbol{\phi} = 20°$)

and active (gain $\neq 0$). It is evident from the figure that the active **ACLD** patches have a significant effect on the control of nonlinear transient vibrations and improve the damping characteristics of the overall panel over the passive damping. The control voltage corresponding to the gain used is quite nominal as shown in Fig. 6. Since the control voltage is proportional to the velocity at the center of the plate, the illustration of control voltage in Fig. 6 indicates that the panel velocity at any point of the overall panel also decays with time. The transient response for a simply supported antisymmetric cross-ply (0°/90°/0°/90°) substrate panel having shallowness angle $\boldsymbol{\phi} = 20°$ is illustrated in Fig. 7. It can be shown that, in this case also, the **ACLD** patches effectively control the nonlinear vibrations of the panel, enhancing the damping characteristics of the panel with low control voltage.

Next, the effect of the variation in shallowness angle on the nonlinear transient responses is studied. Figure 8 illustrates the controlled nonlinear dynamic transient responses of a simply supported laminated cylindrical composite panel for various values of shallowness angle of the panel. Since the overall stiffness of the panel increases with the increase in shallowness angle of the panel, the settling time for the controlled responses of the panel with higher shallowness angle is less than that of the panel with smaller shallowness angle. Similar results are also obtained for symmetric cross-ply and antisymmetric angle-ply panels and for the sake of brevity are not presented here.

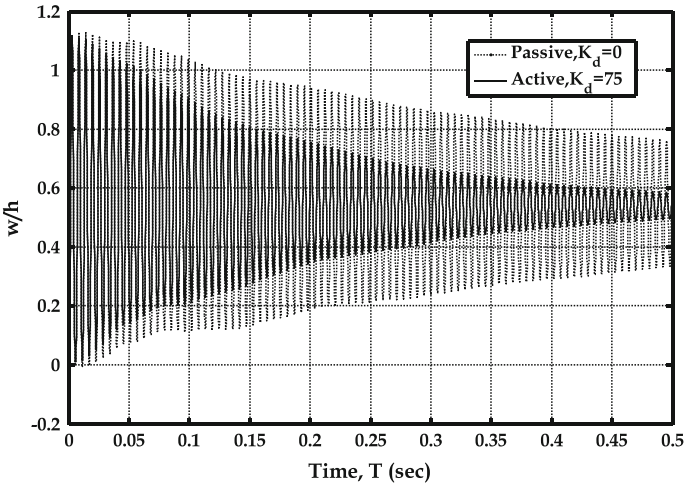

Fig. 7 Nonlinear dynamic responses of a simply supported antisymmetric cross-ply (0°/90°/0°/90°) panel undergoing ACLD ($\mathbf{Q} = 750$, $\boldsymbol{\phi} = 20°$)

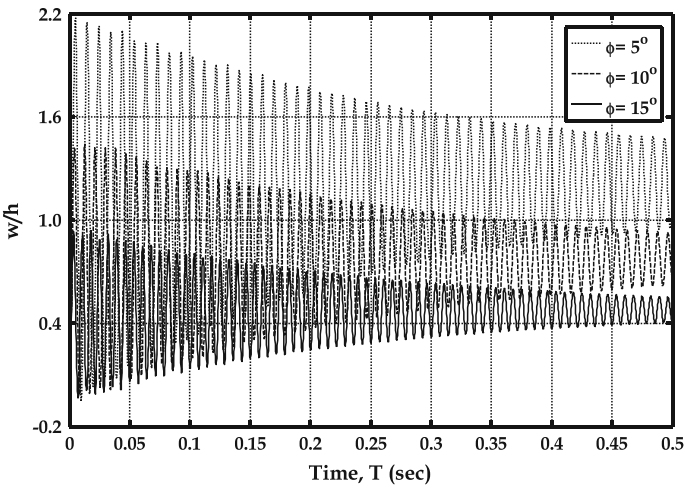

Fig. 8 Comparison of controlled nonlinear dynamic responses of simply supported antisymmetric cross-ply (0°/90°/0°/90°) panel undergoing ACLD for different $\boldsymbol{\phi}$, shallowness angle ($\mathbf{Q} = 400$, $\mathbf{K_d} = 75$)

5 Conclusions

In this paper, a three-dimensional finite element analysis has been carried out to investigate the performance of the patches of **ACLD** treatment for controlling geometrically nonlinear vibrations of thin cylindrical laminated composite panels. The constraining layer of the ACLD patches is considered to be made of the **PFRC** material. The kinematics of deformation of the overall plate is assumed to be based on the first-order shear deformation theory (**FSDT**), and the Von Kármán type strain-displacement relations are used for modeling geometric nonlinearity. The mechanics of the viscoelastic material layer is modeled using the **GHM** approach, which is a time-domain formulation. A simple velocity feedback control loop is used to introduce active damping. Both symmetric and antisymmetric substrates are considered for evaluation of the numerical results. The numerical results demonstrate the use of **ACLD** patches in achieving the active damping to suppress the geometrically nonlinear transient vibrations of the panel effectively. The effect of the shallowness angle on the nonlinear transient response analysis also has been studied. Performance of the activated **ACLD** patches increases with the increase in the value of the shallowness angle for controlling the geometrically nonlinear vibrations of laminated composite panels.

References

1. Bailey, T., Hubbard, J.E.: Distributed piezoelectric polymer active vibration control of a cantilever beam. J. Guid. Control Dyn. **8**, 605–611 (1985)
2. Baz, A., Poh, S.: Performance of an active control system with piezoelectric actuators. J. Sound Vib. **126**, 327–343 (1988)
3. Lee, C.K., Chiang, W.W., Sulivan, O.: Piezoelectric modal sensor/actuator pairs for critical active damping vibration control. J. Acoust. Soc. Am. **90**(1), 374–384 (1991)
4. Hanagud, S., Obal, M.W., Calise, A.J.: Optimal vibration control by the use of piezoceramic sensors and actuators. J. Guid. Control Dyn. **15**(5), 1199–1206 (1992)
5. Devasia, S., Tesfay, M., Padu, B., Bayo, E.A.J.: Piezoelectric actuator design for vibration suppression: placement and sizing. J. Guid. Control Dyn. **16**, 859–864 (1993)
6. Gu, Y., Clark, R.L., Fuller, C.R.: Experiments on active control of plate vibration using piezoelectric actuators and polyvinylidene fluoride modal sensors. J. Vib. Acoust. **116**, 303–308 (1994)
7. Kim, J., Varadan, V.V., V., K., Bao, X.Q.: Finite element modeling of a smart cantilever plate and comparison with experiments. Smart Mater. Struct. **5**(2), 165–170 (1996)
8. Heyliger, P.: Exact solutions for simply supported laminated piezoelectric plates. ASME J. Appl. Mech. **64**, 299–306 (1997)
9. He, L.H.: Axisymmetric response of circular plates with piezoelectric layers: an exact solution. Int. J. Mech. Sci. **40**(12), 1265–1279 (1998)
10. Vel, S.S., Batra, R.C.: Exact solution for rectangular sandwich plates with embedded piezoelectric hear actuators. AIAA J. **39**(7), 1363–1373 (2001)
11. Irschick, H.: A review on static and dynamic shape control of structures by piezoelectric and actuators. Eng. Struct. **24**(1), 5–11 (2002)
12. Ray, M.C.: Optimal control of laminated shells with piezoelectric sensor and actuator layers. AIAA J. **41**, 1151–1157 (2003)
13. Xu, S.X., Koko, T.S.: Finite element analysis and design of actively controlled piezoelectric smart structures. Finite Elements Anal. Des. **40**(3), 241–262 (2004)
14. Peng, F., Ng, A., Hu, Y.R.: Actuator placement optimization and adaptive vibration control of plate smart structures. J. Intell. Mater. Syst. Struct. **16**, 263–271 (2005)
15. Meng, G., Ye, L., Dong, X.J., Wei, K.X.: Closed loop finite element modeling of piezoelectric smart structures. Shock Vib. **13**(1), 1–12 (2006)
16. Kumari, P., Nath, J.K., Dumir, P.C., Kapuria, S.: 2D exact solutions for flat hybrid piezoelectric and magnetoelastic angle-ply panels under harmonic load. Smart Mater. Struct. **16**(5), 1651–1661 (2007)
17. Kwak, M.K., Heo, S., Jeong, M.: Dynamic modeling and active vibration controller design for a cylindrical shell equipped with piezoelectric sensors and actuators. J. Sound Vib. **321**, 510–524 (2009)
18. Balamurugan, V., Narayanan, S.: Finite element modeling of stiffened piezolaminated plates and shells with piezoelectric layers for active vibration control. Smart Mater. Struct. **19**, 105003 (2010)
19. Baz, A.: Active constrained layer damping. U.S. patent 5,485,053 (1996)
20. Baz, A., Ro, J.: Vibration control of plates with active constrained layer damping. Smart Mater. Struct. **5**, 135–144 (1996)
21. Ray, M.C., Baz, A.: Optimization of energy dissipation of active constrained layer damping treatment of plates. J. Sound Vib. **208**, 391–406 (1997)
22. Ray, M.C., Baz, A.: Control of nonlinear vibration of beams using active constrained layer damping treatment. J. Vib. Control **7**, 539–549 (2001)
23. Ray, M.C., Oh, J., Baz, A.: Active constrained layer damping of thin cylindrical shells. J. Sound Vib. **240**(5), 921–935 (2001)
24. Chantalakhana, C., Stanway, R.: Active constrained layer damping of clamped-clamped plate vibrations. J. Sound Vib. **241**(5), 755–777 (2001)
25. Ro, J, Baz, A.: Optimum placement and control of active constrained layer damping using modal strain energy approach. J. Vib. Control **8**, 861–876 (2002)
26. Ray, M.C., Pradhan, A.K.: Active damping of laminated thin cylindrical composite panels using vertically/obliquely reinforced 1-3 piezoelectric composites. Acta Mech. **209**(3–4), 201–218 (2010). doi:10.1007/s00707-009-0149-4
27. Mallik, N., Ray, M.C.: Effective coefficients of piezoelectric fiber reinforced composites. AIAA J. **41**(4), 704–710 (2003)
28. Ray, M.C., Mallik, N.: Performance of smart damping treatment using piezoelectric fiber reinforced composites. AIAA J. **43**(1), 184–193 (2005)
29. Ray, M.C., Shivakumar, J.: Active constrained layer damping of geometrically nonlinear transient vibrations of composite plates using piezoelectric fiber-reinforced composite. Thin-Walled Struct. **47**, 178–189 (2009)
30. Panda, S., Ray, M.C.: Active constrained layer damping of geometrically nonlinear vibrations of functionally graded plates using piezoelectric fiber reinforced composites. Smart Mater. Struct. **17**(2), 1–15 (2008)
31. Sarangi, S.K., Ray, M.C.: Smart damping of geometrically nonlinear vibrations of laminated composite beams using vertically reinforced 1-3 piezoelectric composites. Smart Mater. Struct. **19**, 075020 (2010)
32. Sarangi, S.K., Ray, M.C.: Active damping of geometrically nonlinear vibrations of laminated composite plates using vertically/obliquely reinforced 1-3 piezoelectric composites. Acta Mech. **222**(3–4), 363–380 (2011). doi:10.1007/s00707-011-0531-x
33. Sarangi, S.K., Ray, M.C.: Active damping of geometrically nonlinear vibrations of laminated composite shallow shells using vertically/obliquely reinforced 1-3 piezoelectric composites. Int. J. Mech. Mater. Des. **7**(1), 29–44 (2011)
34. Reddy, J.N., Chandrashekara, K.: Nonlinear analysis of laminated shells including transverse shear strains. AIAA J. **23**, 40–41 (1985)
35. Kundu, C.K., Han, J.H.: Nonlinear buckling analysis of hygrothermoelastic composite shell panels using finite element method. Composites B **40**, 313–328 (2009)
36. Lam, M.J., Inman, D.J., Saunders, W.R.: Hybrid damping models using the Golla_hughes-McTavish method with internally balanced model reduction and output feedback. Smart Mater. Struct. **9**, 362–371 (2000)
37. Mc Tavish, D.J., Hughes, P.C.: Modeling of linear viscoelastic space structures. J. Vib. Acoust. **115** (1993), 103–113

38. Lim, Y.-H., Varadan, V.V., Varadan, K.K.: Closed loop finite element modeling of active constrained layer damping in the time domain analysis. Smart Mater. Struct. **11**, 89–97 (2002)
39. Reddy, J.N.: Geometrically nonlinear transient analysis of laminated composite plates. AIAA J. **21**(4), 621–629 (1983)